FFI Norwegian Defence Research Establishment

22/01379

FFI-RAPPORT

Estimation of orientation of an aircraft using position data only

Emil B. Kalveland

Estimation of orientation of an aircraft using position data only

Emil B. Kalveland

Norwegian Defence Research Establishment (FFI) 26 September 2022

Keywords
Estimering
Navigasjon
Satellittnavigasjon
Radar
Fly

FFI report
22/01379

Project number
1557

Electronic ISBN
978-82-469-3425-4

Approvers
Tore Ulversøy, *Research Manager*
Tor-Odd Høydal, *Director of Research*
Kenneth Gade, *Principal Scientist*

The document is electronically approved and therefore has no handwritten signature.

Summary

This report introduces a method for estimation of an aircraft's orientation on the basis of measurements of its position only. Typical sources for the position data is global navigation satellite systems or radar measurements. The orientation estimation is based on certain assumptions regarding the aircraft's maneuvering, mainly coordinated flight, constant wind and partly constant true airspeed.

For heading estimation, the method involves estimation of the winds aloft to compensate for aircraft crab in the horizontal plane.

The proposed method is described mathematically, followed by an example of application on GPS data from 30 minutes of flight of a C-130J aircraft.

In the example, the difference between the estimations and reference measurements for all axes had a standard deviation of around one degree or less.

The method does not account for angle of attack, which reduces accuracy of the pitch estimates in general and the heading estimates during maneuvering. Roll estimates and heading estimates when flying straight are not significantly affected.

Sammendrag

Denne rapporten introduserer en metode for å bedømme et flys orientering, med utgangspunkt i posisjonsmålinger alene. Typiske kilder for disse posisjonsmålingene kan være satellittnavigasjon eller radar. Estimeringen baserer seg på definerte forutsetninger, hovedsakelig koordinert flygning, konstant vind og delvis konstant flyhastighet.

Den foreslåtte metoden inkluderer estimering av høydevinden rundt flyet, og kompenserer for denne når retningen i horisontalplanet skal bedømmes.

Rapporten inneholder først en matematisk beskrivelse av metoden. Deretter følger et eksempel på praktisk bruk. Eksempelet viser orienteringsbedømming for et fly av typen C-130J, basert på posisjonsdata fra satellittnavigasjon.

I eksempelet blir orienteringsestimatet sammenlignet med en referansemåling. Forskjellen er liten. Skillet mellom estimatet og referansemålingen for alle tre aksene viser et standardavvik på rundt en grad eller mindre.

Metoden tar ikke hensyns til flyets angrepsvinkel. Dette reduserer estimatets nøyaktighet for pitch generelt, og for yaw under manøvrering. Estimatet av roll-vinkelen generelt, og retning når flyet ikke manøvrerer, blir ikke påvirket nevneverdig av dette.

Contents

1 Introduction

When doing analysis on data involving maneuvering aircraft, some problems require knowledge of the aircraft's orientation. Even though most modern commercial and military aircraft carry highly precise inertial navigation systems measuring orientation, that data is not always available for analysis. Some aircraft lack the means to record and extract such information after flight, and some use cases might involve processing data from non-cooperating aircraft, like random targets being tracked by a radar.

This text proposes a method to estimate orientation of an aircraft when direct orientation measurements are not available. The method assumes that position or velocity data is available, for instance from a global navigation satellite system (GNSS), radar or other kinds of tracking sensors. In addition, the method is based on certain assumptions regarding the maneuvering of the aircraft and wind conditions.

Chapter 2 presents the method, while chapter 3 shows an example of how the method could be applied to real data. The example shows what level of accuracy to expect from the method, the method's weaknesses and how to consider the pertinent assumptions for the given circumstances. Chapter 4 summarizes the most important results from the previous chapters.

2 Method for estimation of orientation

The proposed method estimates an aircraft's orientation using position or velocity data, and a set of given assumptions. The method also gives estimates for the current wind around the aircraft and its true airspeed.

As the title suggests, the starting point of the method is position data. However, the actual data needed is velocity data in a navigational frame, which can be derived from position data by numerical differentiation.

2.1 Assumptions

The method is based on the following assumptions:

- Constant wind
- Constant true airspeed
- Coordinated flight

The assumptions will never be completely fulfilled in real situations. The accuracy and precision of the estimations are affected by how well the assumptions match reality. To apply the method to real data, it is crucial to understand how these assumptions affect the estimates, and if that makes the proposed method useful for your particular use case.

A more detailed description of each assumption follows.

2.1.1 Constant wind

We assume that the wind is constant, with no vertical components and no whirlwind, i.e. the air mass is not rotating relative to the earth. This assumption needs to be valid for the entire dataset.

2.1.2 Constant true airspeed

True airspeed is the speed of an aircraft relative to the air mass surrounding it. This assumption only needs to be fulfilled for the parts of the dataset used for wind estimation, described in section 2.5.

2.1.3 Coordinated flight

By coordinated flight in this text, we mean flight with no sideslip. Sideslip is the angle between the longitudinal axis of an aircraft and the oncoming airflow in the horizontal plane.

Coordinated flight is achieved on fixed wing aircraft by appropriate rudder deflection relative to aileron deflection.

When an aircraft is flying coordinated, observers on board will not perceive lateral acceleration and their weight will be acting straight down into their seats.

For many cases, this is a reasonable assumption, as coordinated flight for instance makes manned flights more comfortable and minimizes the drag force on the aircraft.

2.2 Limitations

The method does not account for angle of attack. Section 2.6.1 and 2.7 describe how this affect the heading and pitch estimates. Heading estimation, when flying with wings level, and roll angle

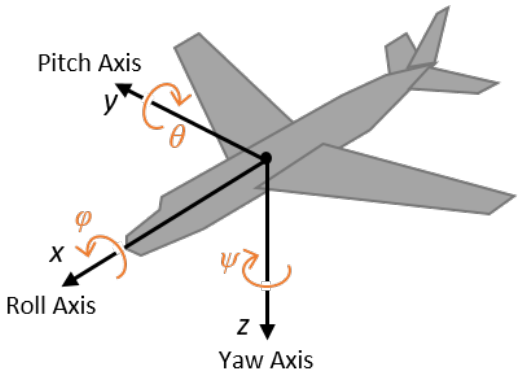

Figure 2.1 The figure shows the axes of the B frame (the aircraft) with notations.

estimation in general are not significantly affected by this limitation. Section 3.7 shows how this affected our experiment, and explores how a simple approximation could minimize the estimates' deviations.

2.3 Notation

Heading, pitch angle and roll angle are presented by ψ, θ and ϕ, as illustrated in figure 2.1. Angles estimated using our proposed method gets a hat, i.e. $\hat{\psi}$, $\hat{\theta}$ and $\hat{\phi}$.

Vectors, frames and rotation matrices are represented using the unified notation proposed by Gade in Chapter 2 of [1], which could be referenced for a thorough description. A short summary of the most used notations, and some notations specific for this text, is outlined below.

2.3.1 Rotation matrices

Rotation matrices in this text follows the notation in [1], i.e. a rotation from arbitrary frame B to arbitrary frame A is written $\mathbf{R}_{AB}$. The relation between a vector $\vec{p}$ represented in frame B and the same vector represented in frame A is:

$$\mathbf{p}^A = \mathbf{R}_{AB}\mathbf{p}^B \tag{2.1}$$

The inverse transformation can be accomplished by transposing the rotation matrix, i.e.

$$\mathbf{R}_{BA} = (\mathbf{R}_{AB})^T \tag{2.2}$$

Some places the rotation matrix is given as a function of three angles, $\mathbf{R}(\psi, \theta, \phi)$. This function represents a rotation about new axes in the zyx order. $\mathbf{R}_{AB} = \mathbf{R}(\psi, \theta, \phi)$ implies that a rotation from A to B is the same as rotating A an angle of ψ around the z axis, then a rotation around the new y axis an angle of θ and finally a rotation about the new x axis an angle of ϕ. This function could be used to transform from a frame fixed to the aircraft, as in figure 2.1, to a north-east-down frame.

2.3.2 Frames

The following frames, commonly used in navigation, are used:

E Earth-fixed.

N North-east-down frame with origin on the earth surface directly below the aircraft.

B Body frame, in our case fixed to the aircraft with axes as in figure 2.1.

W Wind, i.e. the air surrounding the aircraft, modeled as a solid body.

Somewhat unusual frames are defined specifically for our purpose:

Z Frame rotated from frame N to the aircraft's heading, with origin as in B. The rotation from N frame to Z frame is $\mathbf{R}(-\psi, 0, 0)$, where ψ represent aircraft heading.

Y Frame rotated from frame N to the aircraft's heading and pitch, with origin as in B. The rotation from N frame to Y frame is $\mathbf{R}(-\psi, -\theta, 0)$, where ψ represent aircraft heading and θ represent aircraft pitch angle.

2.3.3 Vectors

The letters used to represent vectors are:

p Position

v Velocity

a Acceleration

g Gravity

A few places in the text we use coordinate free vectors, meaning that the vector is not yet decomposed in a defined coordinate system [1]. Coordinate free vectors are mainly used to derive (2.13). They are represented with an arrow above, for instance $\vec{v}$, while an algebraic vector decomposed in frame N is represented in bold with its frame in superscript, like $\mathbf{v}^N$.

The concept of generalized velocity, as defined in [1], is needed to derive (2.12). Readers not familiar with coordinate free vectors or generalized velocity will probably still be able to understand the method proposed in this text, with the exception of the mathematics behind (2.13).

An example of a coordinate free vector, representing the velocity of B (the aircraft) relative to E (the earth), observed from E:

$$\vec{v}_{\underline{E}B} \tag{2.3}$$

If a vector is representing the velocity observed from a different frame than the first frame in the subscript, we can use the notation from [1] for generalized velocity, where E is the frame the derivation is seen from:

$$^{E}\vec{v}_{WB} \tag{2.4}$$

The coordinate-free vector (2.3) decomposed in the N frame:

$$\mathbf{v}^N_{\underline{E}B} \tag{2.5}$$

Scalars in algebraic vectors are represented using normal font letters, with the axis following in the subscript:

$$\mathbf{v}^N_{\underline{E}B} = \begin{bmatrix} v^N_{\underline{E}B,x} \\ v^N_{\underline{E}B,y} \\ v^N_{\underline{E}B,z} \end{bmatrix} \tag{2.6}$$

2.4 Principle for the heading estimation

The proposed method for heading estimation is based on method 6 in [2]. Method 6 assumes that $\vec{v}_{\underline{E}B}$ is known, both decomposed in the body frame B, $\mathbf{v}^B_{\underline{E}B}$, and in the E frame, $\mathbf{v}^E_{\underline{E}B}$. The relation between these two vectors is:

$$\mathbf{v}^E_{\underline{E}B} = \mathbf{R}_{EB}\mathbf{v}^B_{\underline{E}B} \tag{2.7}$$

$\mathbf{R}_{EB}$ is the orientation of the vehicle, which can be calculated from the two vectors. Only the direction of the vectors are needed to calculate the orientation, not the magnitude.

Our method assumes that $\mathbf{v}^E_{\underline{E}B}$ is available, for instance from GNSS or radar measurements. In our text we mainly represent it in the N frame, as $\mathbf{v}^N_{\underline{E}B}$.

Method 6 assumes that $\mathbf{v}^B_{\underline{E}B}$ is available from sensor measurements on board the vehicle, or that the vehicle is assumed to always point in the direction of travel, like a vehicle on rails or wheels. The assumption in the latter case can be described mathematically as

$$\mathbf{v}^B_{\underline{E}B} \approx \begin{bmatrix} x \\ 0 \\ 0 \end{bmatrix} \tag{2.8}$$

where x is the forward speed.

Our method of heading estimation does not assume that we have measurements of $\mathbf{v}^B_{\underline{E}B}$. The assumption of (2.8) in the case of an aircraft could be a gross simplification, depending on aircraft sideslip, angle of attack and winds. The next section describes a method for estimating the winds aloft in the horizontal plane, making us able to estimate the aircraft's horizontal velocity relative to the wind, $\mathbf{v}^N_{\underline{W}B}$. Under our assumptions; coordinated flight (flight with no sideslip), no vertical wind components and disregarding angle of attack, we accept the following approximation:

$$\mathbf{v}^B_{\underline{W}B} \approx \begin{bmatrix} x \\ 0 \\ 0 \end{bmatrix} \tag{2.9}$$

Heading estimation then boils down to finding the direction of $\mathbf{v}^N_{\underline{W}B}$ in the horizontal plane.

2.5 Estimating wind from velocity data

To find an estimate for the heading, we first need to find an estimate for the wind velocity around the aircraft. This section describes how to estimate the wind velocity, and the relations between velocity vectors representing heading / true airspeed, course / groundspeed and wind velocity.

The three velocity vectors are illustrated in figure 2.2, where we can see that the heading / true airspeed vector and the wind velocity vector added together equals the course / groundspeed vector. This simple relationship is not true in general for velocities, but it holds as long as the velocities (derivations) are seen from the same frame. When all velocities are seen from the E frame, we can write the relation using notation for generalized velocity and cancel intermediate coordinate frames [1, equation 2.36]:

$${}^E\vec{v}_{EB} = {}^E\vec{v}_{EW} + {}^E\vec{v}_{WB} \tag{2.10}$$

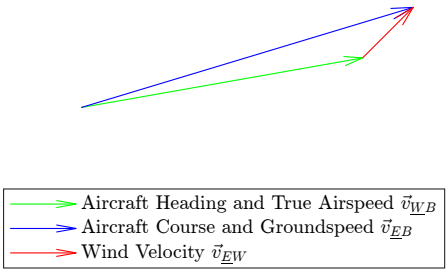

Figure 2.2 Relation between velocity vectors representing heading / true airspeed, course / groundspeed and wind, in accordance with (2.12).

Our assumption of no whirlwind, i.e. $\vec{\omega}_{EW} = 0$, implies that there is no angular velocity between frame E and W, which means that the velocity seen from E is equal to the velocity seen from W:

$$^{W}\vec{v}_{WB} = {}^{E}\vec{v}_{WB} \tag{2.11}$$

Now we can use standard velocity and rewrite (2.10):

$$\vec{v}_{\underline{E}B} = \vec{v}_{\underline{E}W} + \vec{v}_{\underline{W}B} \tag{2.12}$$

When we decompose in frame N and solve for $\mathbf{v}^N_{\underline{W}B}$, we get the following relation:

$$\mathbf{v}^N_{\underline{W}B} = \mathbf{v}^N_{\underline{E}B} - \mathbf{v}^N_{\underline{E}W} \tag{2.13}$$

Let's take a look at how the vectors in (2.13) are connected geometrically in the horizontal plane under our assumption of constant true airspeed and constant wind. First, consider the heading / true airspeed vectors, $\mathbf{v}^N_{\underline{W}B}$, for an aircraft flying in a circle with constant airspeed. Figure 2.3 shows vectors for different headings. The tip of the vectors resemble a circle with radius equal to true airspeed, disregarding vertical movement. The circle can be described mathematically by:

$$\left(v^N_{\underline{W}B,x}\right)^2 + \left(v^N_{\underline{W}B,y}\right)^2 = v_{ta}^2 \tag{2.14}$$

v_{ta} geometrically is the circle's radius, which corresponds to true airspeed in the horizontal plane and is described by:

$$v_{ta} = \sqrt{\left(v^N_{\underline{W}B,x}\right)^2 + \left(v^N_{\underline{W}B,y}\right)^2} \tag{2.15}$$

Let's continue our visual reasoning from figure 2.3, and add wind to all the heading / true airspeed vectors. Figure 2.4 shows how the resulting course / groundspeed vectors, $\mathbf{v}^N_{\underline{E}B}$, resembles an offset circle when a constant wind vector is added. In figure 2.5 only the resulting circles are shown, illustrating how the circles are offset by the wind vector. Note that as long as the wind is constant, the shape and size of the circles are equal.

We use the relationship in (2.13) and expand (2.14):

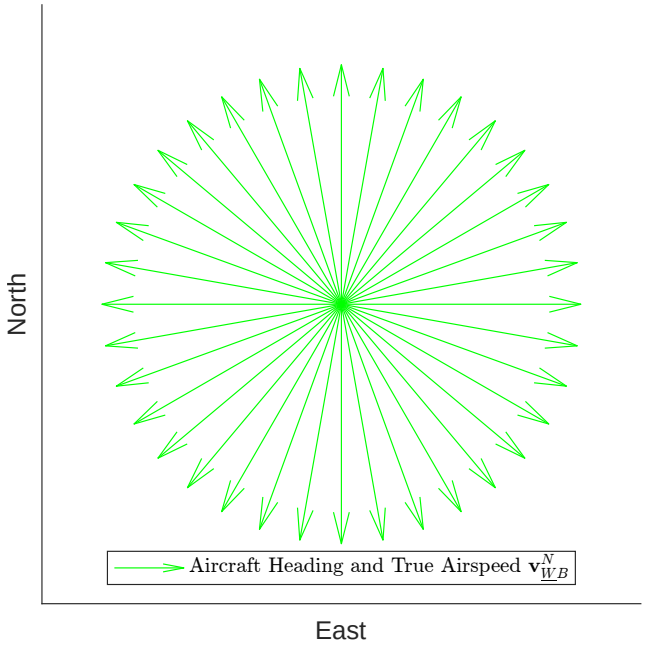

Figure 2.3 Vectors representing heading and true airspeed. The airspeed is constant, while the heading is changing. The tip of the vectors draw a circle in the north-east-plane.

$$(v^N_{\underline{E}B,x} - v^N_{\underline{E}W,x})^2 + (v^N_{\underline{E}B,y} - v^N_{\underline{E}W,y})^2 = v^2_{ta} \tag{2.16}$$

Our assumptions of constant true airspeed and constant wind, implies that the x and y components of $\mathbf{v}^N_{\underline{E}W}$ and v_{ta} in (2.16) are constant. Position/velocity data from a flight gives us a potentially large set of values for $\mathbf{v}^N_{\underline{E}B}$. Estimation of the constants can be found by optimization, for instance by a nonlinear least squares curve-fitting algorithm, which will find wind components and the value for true airspeed which minimizes each velocity sample's distance from a perfect circle.

The distance for each $\mathbf{v}^N_{\underline{E}B}$ sample to the circle, i.e. the distance that should be minimized, is given by:

$$distance = \sqrt{(v^N_{\underline{E}B,x} - v^N_{\underline{E}W,x})^2 + (v^N_{\underline{E}B,y} - v^N_{\underline{E}W,y})^2} - v_{ta} \tag{2.17}$$

2.6 Estimating heading

Having estimated the wind, we use the relation of (2.13) to calculate $\mathbf{v}^N_{\underline{W}B}$.

For an aircraft flying with its wings level and no sideslip, the heading of the aircraft is the angle between true north and the heading / true airspeed vector $\mathbf{v}^N_{\underline{W}B}$ in the horizontal plane, as illustrated in figure 2.6. This angle could be found using the well known atan2 function:

$$\hat{\psi} = \text{atan2}\left(v^N_{\underline{W}B,y}, v^N_{\underline{W}B,x}\right) \tag{2.18}$$

When the aircraft is not flying with its wings level, i.e. the roll angle is not equal to zero, the

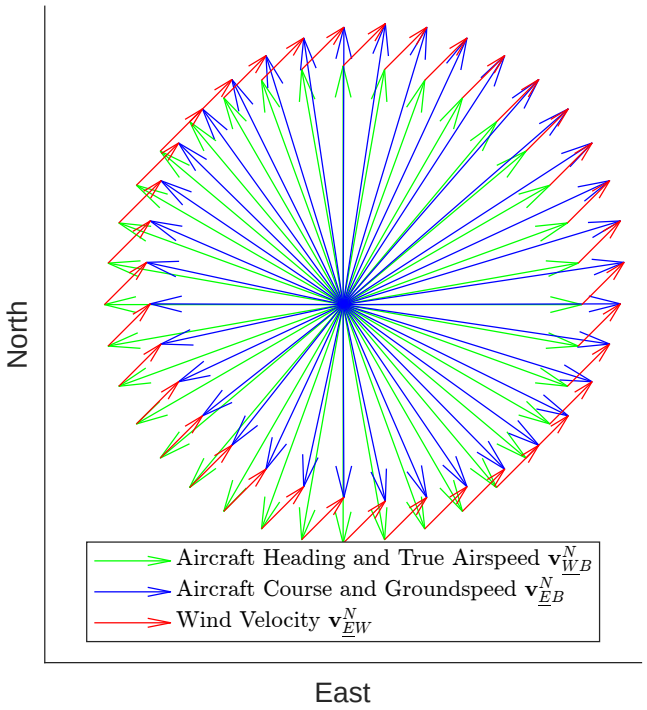

Figure 2.4 Relation between velocity vectors representing course, heading and wind. The wind and true airspeed is constant, but the heading changes. The tip of the blue velocity vectors draw an offset circle in the north-east plane.

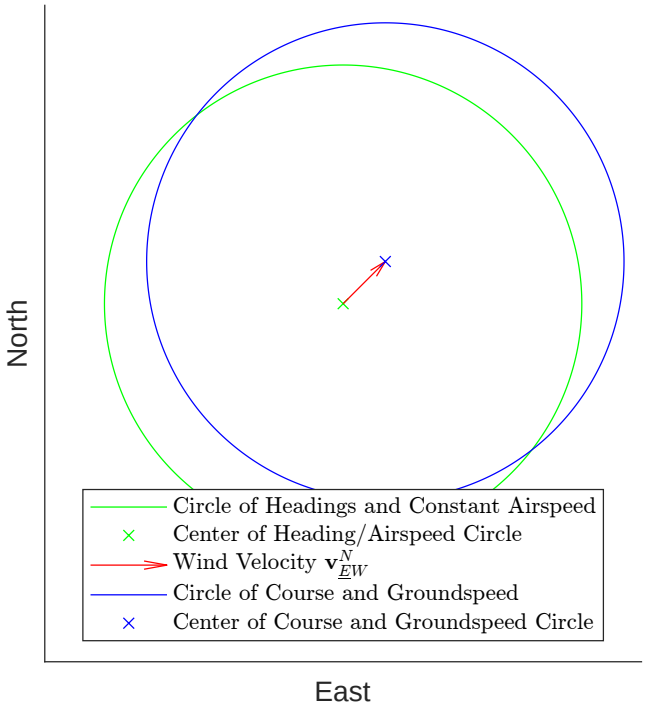

Figure 2.5 The tip of the green and blue vectors in figure 2.4 presented as circles. The centers of the circles are offset by the wind vector.

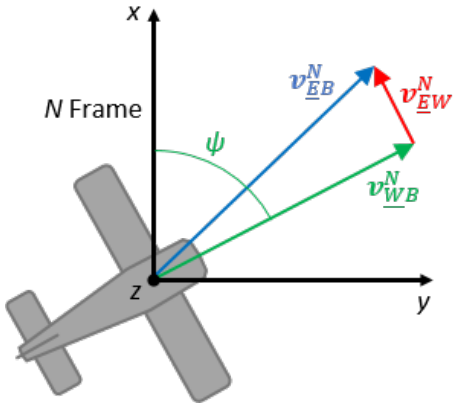

Figure 2.6 Under the assumptions described in the text, the aircraft's heading is the angle between the x axis in the N frame and the $\mathbf{v}^N_{\underline{W}B}$ *vector in the horizontal plane.*

angle of attack will affect the heading, and the above relation will be inaccurate. Our proposed method does not account for the angle of attack.

2.6.1 Ramification of not accounting for the angle of attack

Angle of attack is the angle between a defined longitudinal axis of an aircraft and the flight path vector, as depicted in figure 2.7. For an aircraft flying with its wings level, the plane of the angle of attack will be perpendicular to the horizontal plane, and therefore not affect our heading estimate.

As soon as the aircraft starts to roll, the angle of attack will be projected into the horizontal plane. The angle of attack will then make our estimate of heading lag compared to the real heading in a turn.

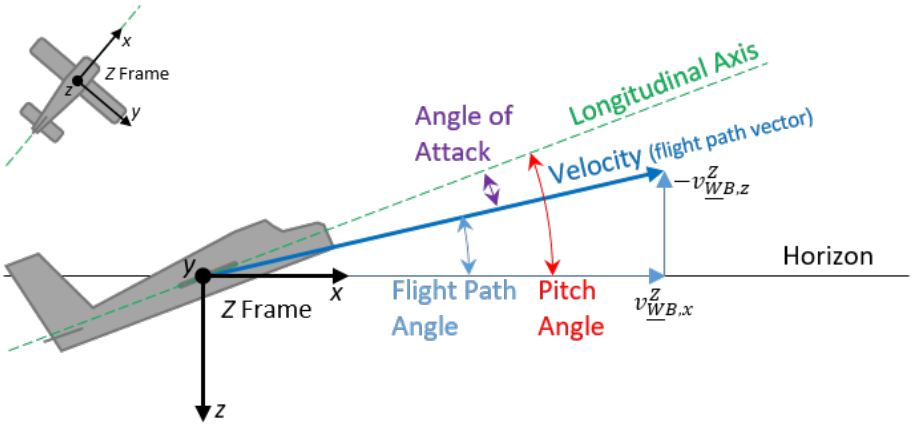

Figure 2.7 Relation between pitch, flight path angle and angle of attack.

2.7 Estimating the pitch angle

As illustrated in figure 2.7, the pitch angle is the sum of the flight path angle and the angle of attack, but our estimation only provides the flight path angle. Angle of attack varies significantly throughout a flight, and anyone using this method will have to consider whether an estimate that disregards angle of attack will be sufficient for their needs. More about how angle of attack varies with flight, how it affects our estimate and an example of how an approximation of angle of attack can be used together with our proposed method are provided in section 3.7.

To calculate the flight path angle, we represent $\mathbf{v}^N_{\underline{WB}}$ in frame Z and calculate the angle based on the x and z components of $\mathbf{v}^Z_{\underline{WB}}$. We use our previously calculated heading estimate, $\hat{\psi}$, to represent the vector in the Z frame:

$$\mathbf{v}^Z_{\underline{WB}} = \mathbf{R}_{ZN}\mathbf{v}^N_{\underline{WB}} = \mathbf{R}(-\hat{\psi}, 0, 0)\mathbf{v}^N_{\underline{WB}} \tag{2.19}$$

By our simplification, disregarding the angle of attack completely, the pitch angle is equal to the flight path angle, which is found from the x and z components by the following function:

$$\hat{\theta} = -\operatorname{atan2}\left(v^Z_{\underline{WB},z}, v^Z_{\underline{WB},x}\right) \tag{2.20}$$

2.8 Estimating the roll angle

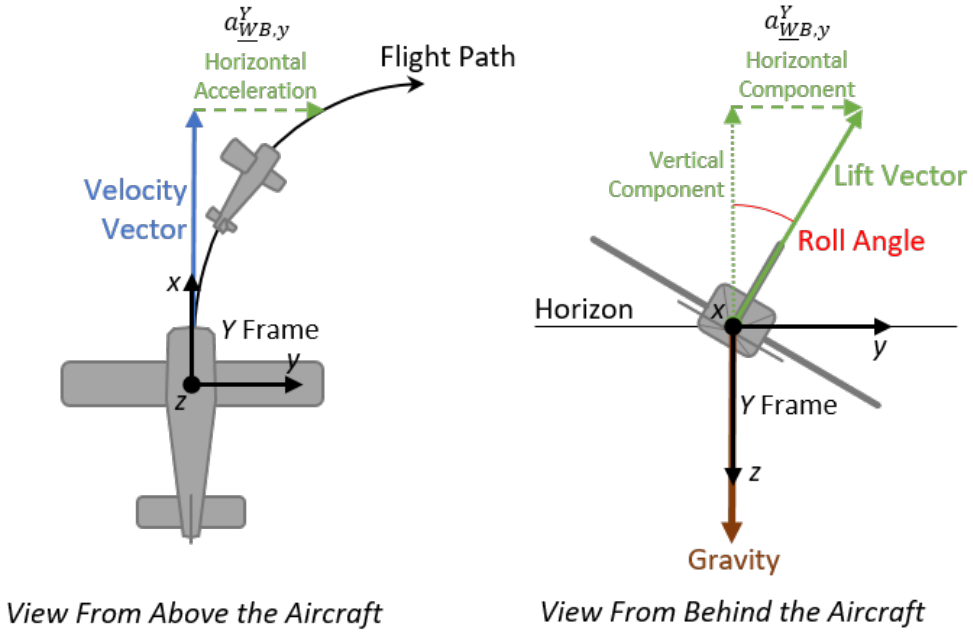

Figure 2.8 Relation between horizontal acceleration and roll angle for coordinated, level flight.

The horizontal component of the lift vector, $a^Y_{\underline{WB},y}$, is the acceleration that changes the velocity vector of the aircraft during a turn, as illustrated to the left in figure 2.8. Our assumption of

coordinated flight gives the relation of forces as shown to the right in the figure, with the roll angle as the angle between the lift vector and its vertical component. To calculate the angle, we first need to find $\mathbf{a}^Y_{\underline{W}B}$.

Our assumption of no whirlwind makes the following relation true, as discussed for velocity in section 2.5:

$$\mathbf{a}^N_{\underline{E}B} = \mathbf{a}^N_{\underline{E}W} + \mathbf{a}^N_{\underline{W}B} \tag{2.21}$$

The assumption of constant wind constitutes that the wind does not have an acceleration, i.e. $\mathbf{a}^N_{\underline{E}W} = 0$, which means that $\mathbf{a}^N_{\underline{E}B} = \mathbf{a}^N_{\underline{W}B}$ in accordance with (2.21).

We can find $\mathbf{a}^N_{\underline{W}B} = \mathbf{a}^N_{\underline{E}B}$ by numerical differentiation of $\mathbf{v}^N_{\underline{E}B}$. The acceleration can then be presented in frame Y by the following rotation, using our previous estimates for heading and pitch angle:

$$\mathbf{a}^Y_{\underline{W}B} = \mathbf{R}_{YN}\mathbf{a}^N_{\underline{W}B} = \mathbf{R}(-\hat{\psi}, -\hat{\theta}, 0)\mathbf{a}^N_{\underline{W}B} \tag{2.22}$$

With the acceleration represented in frame Y, the roll angle can be calculated by the following function, where $|\vec{g}|$ denotes the gravity constant:

$$\hat{\phi} = \text{atan2}\left(a^Y_{\underline{W}B,y}, |\vec{g}| - a^Y_{\underline{W}B,z}\right) \tag{2.23}$$

3 Applying the method to real data

The intention of this chapter is to give the reader a practical example of how the proposed method can be applied, its limitations and expected performance.

The proposed method was tested on real data recorded on board a C-130J during parts of a four hours long flight with a significant amount of maneuvering. The results were compared to orientation measurements from an FFI developed instrument, referred to as "navsystem" in this text.

This chapter also contains a section "Compensating for Angle of Attack", which shows how the proposed method could produce more precise data if a function approximating the angle of attack is available.

3.1 Test equipment

The navsystem providing orientation measurements consists of an IMU and a GPS. Data from the sensors was recorded throughout the flight. The data was then post-processed using NavLab [3], which estimates the orientation based on acceleration measurements from the IMU and data from the GPS, using the principle described as method 7 in [2]. NavLab also provided smoothing of the orientation and the position data.

The navsystem was fixed to a table in the cockpit of the aircraft, assumed to be representing the plane of the pitch and roll axes of the aircraft.

3.2 Observed surface winds

The surface winds at Andøya were light during the flight, as seen in figure 3.1. The surface winds are not expected to be equal to the winds aloft, but historical data on winds aloft were not available. The data still serves as a general reference of the wind conditions that day. Normally, winds aloft are stronger than the surface winds because winds near the surface are slowed by friction. The lower wind speed near the surface also limits the effect of the Coriolis force, which means that a slight difference in wind direction is expected between the surface winds and the winds aloft.

3.3 Dataset

The dataset included position (latitude, longitude and altitude) and orientation (heading, pitch and roll) timestamped with an average sample rate of 100 samples per second.

Recording started with the aircraft in the air at about 68°30′ N in transit northbound, and ended with landing at Andøya Airport. Time of the first sample was 09:51:02, while the time of the last sample was 14:00:56. Figure 3.2 shows the flight path of the aircraft.

As described in chapter 2, the proposed method assumes constant wind and coordinated flight, in addition to constant true airspeed for the part of the dataset used to estimate the wind.

Winds aloft tend to change with altitude, geographical area and time. To increase the chance of fulfilling the assumption of constant wind, we restricted the dataset to only include the part from 13:00 to 13:30. The surface wind was relatively stable during that time segment, and the aircraft maneuvered in a limited geographical area at a constant altitude of about 800 meters.

The position data was differentiated numerically twice (without smoothing), to obtain velocity and acceleration vectors at all time samples.

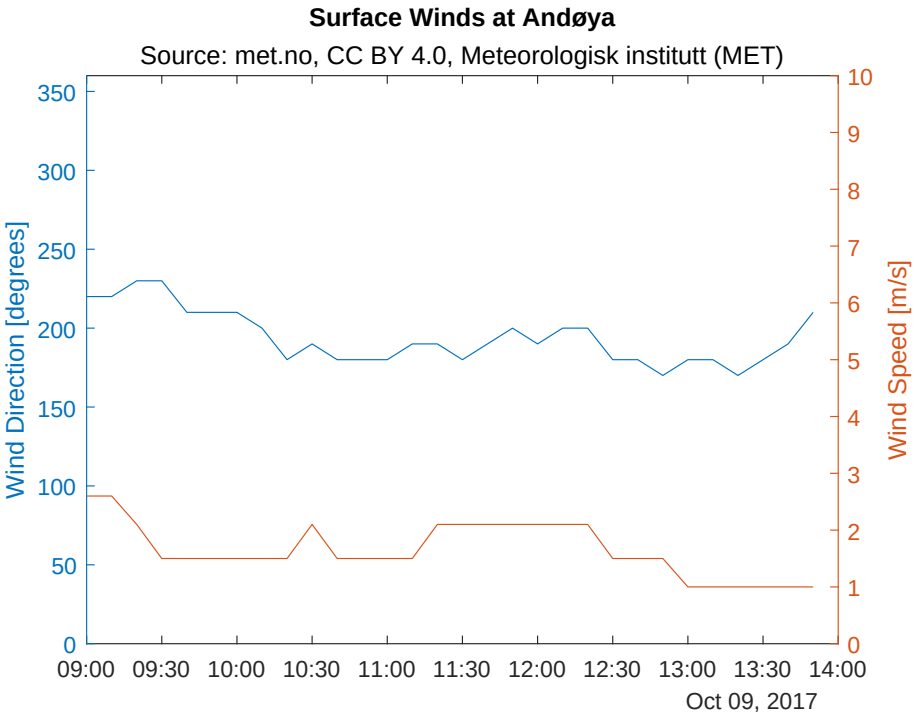

Figure 3.1 Observed surface winds at Andøya for the time of the experiment.

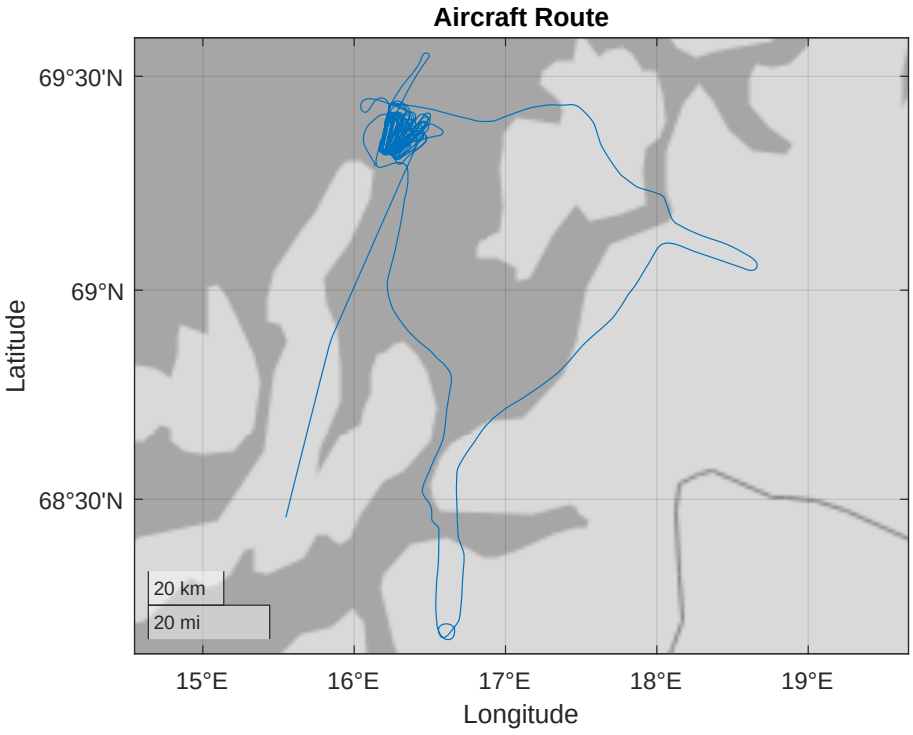

Figure 3.2 Flight path from the full dataset.

3.3.1 Calibrating orientation data from the navsystem

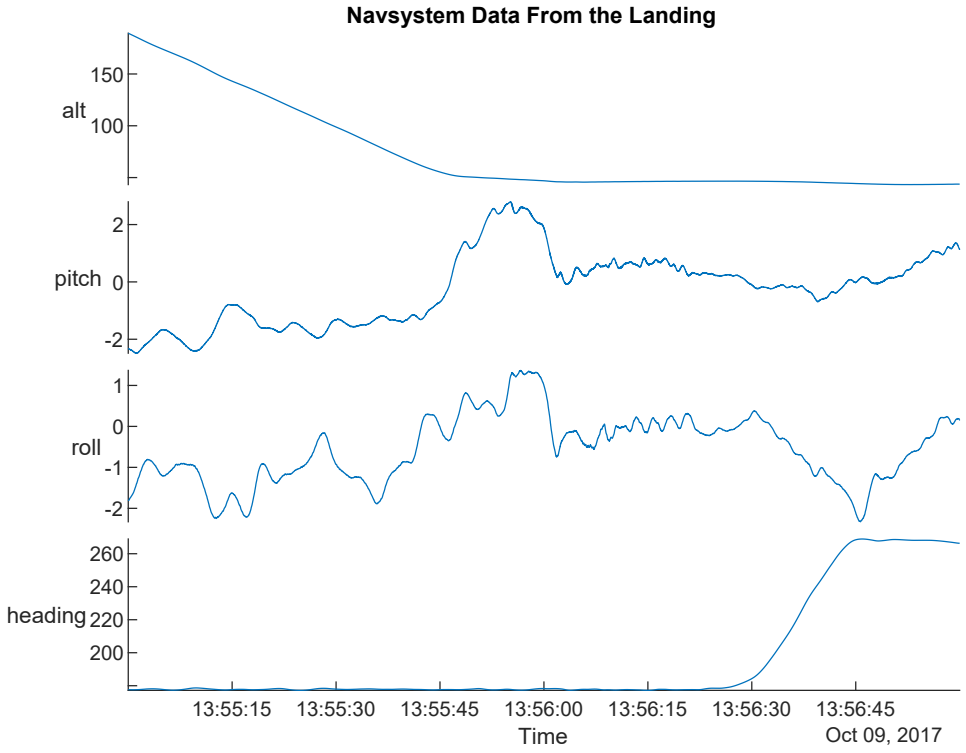

Figure 3.3 Navsystem data showing altitude and orientation during landing.

The orientation of the navsystem around the yaw axis relative to the aircraft was not known. To find the offset in heading between the aircraft and the navsystem, we used two different methods. Both methods were based on comparing the heading of the navsystem with the course of the aircraft rolling down the runway after landing, when the aerodynamic forces no longer affected the orientation of the aircraft. We assume that (2.8) holds for this part of the dataset, as the aircraft's direction of travel now is wheel based.

In the first method, we compared the true bearing of the runway with the navsystem heading, assuming that the pilots maneuvered along or parallel to the centerline of the runway. The other method used velocity data derived from the GPS as a reference for the course of the aircraft.

To find out when the aerodynamic forces no longer were dominant on the aircraft, we plotted navsystem altitude, pitch, roll and heading from the last part of the flight, see figure 3.3. From the plot we assessed touchdown at 13:56:03, and start of turn to leave the runway at 13:56:23.

For the first method, we calculated the mean heading from the time in-between, leaving 3 seconds in each end as a buffer, indicating a heading offset between the aircraft and the navsystem of 27.84°.

Using the second method, we calculated an offset of 27.77°.

The result of the second method was used to calculate a rotation matrix to update the orientation data from the navsystem to represent the aircraft's orientation. These data was used throughout this chapter as a reference for orientation. Angles from the navsystem are denoted without a hat, i.e. ψ, θ and ϕ.

3.4 Heading estimation

We estimated the heading using two methods, the proposed method using the assumption in (2.9) and a simpler method not regarding the winds, following the assumption in (2.8). Both methods were compared to the navsystem heading.

3.4.1 Estimating heading from course alone

First, we estimated the aircraft heading from course alone. By course alone, we mean using the previously referenced method 6 from [2], under the assumption that the aircraft always points in the direction it moves, in accordance with the approximation in (2.8). This method does not account for sideslip or wind, but is probably the easiest way of estimating heading using position data. We estimated the heading using this method to get a baseline, prior to using our proposed method.

Figure 3.4 shows the distribution for the estimated heading compared to the navsystem heading. Further details of the distribution are revealed in figure 3.5, where the y-axis indicates the navsystem heading of the aircraft for the samples, in addition to the delta heading as in the histogram above. The figure shows that each of the tops in the histogram represent flight in certain headings, and the delta heading varies by the amount of crosswind flying in a given direction.

3.4.2 Estimating aircraft heading using the proposed method

As described in chapter 2, the proposed method involves estimating the winds aloft to enable a more accurate estimation of the heading.

3.4.2.1 Estimating winds aloft

The method assumes that the winds are constant. By reducing the dataset to a portion of the flight limited in time and space, the likelihood of the winds aloft to be stable for the chosen period is increased.

For the estimation of the winds aloft to be precise when using the proposed method, the true airspeed needs to be constant. To increase the likelihood of the true airspeed to be constant, we limited the dataset used for wind estimation to only include samples where the double derivative of the position, $\left|\vec{a}_{\underline{E}B}\right|$, were less than 1 m/s. This excludes varying airspeed related to maneuvering from the dataset, in addition to limit the effect of angle of attack during turns, as described in section 2.6.1. Tracks from the limited dataset are shown in figure 3.6.

Using the limited dataset, we estimated the wind using the method from section 2.5, giving a result of 3.7 m/s from 169.6°. Figure 3.7 shows a scatter plot of the data, and the curve fitted circle. The slight offset of the red circle's center from the origin represents the wind vector.

3.4.2.2 Estimating heading

Having calculated the wind, we estimated the heading for each sample in the dataset using equation 2.18. Figure 3.8 shows the estimated headings compared to the navsystem headings. The accuracy of the estimate is expected to decrease when the aircraft is in a turn due to the angle of attack. To see how the estimate performs during straight and level flight, we also plotted a histogram of the heading estimate from samples having g-force around one in the aircraft z-axis. The figure shows a significant difference in accuracy of the samples from steady flight, compared to maneuvering flight.

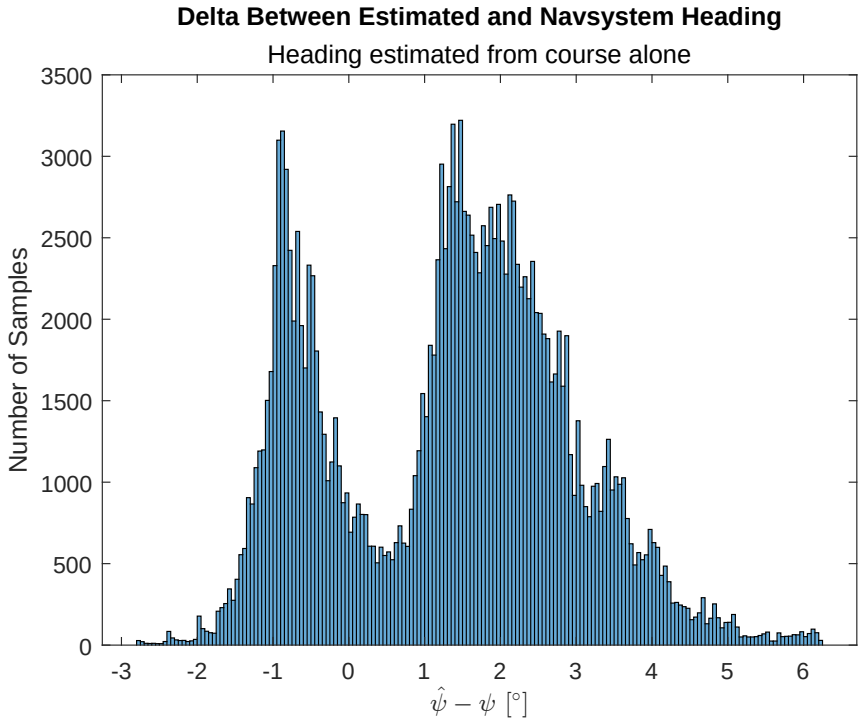

Figure 3.4 Distribution of all samples in the dataset (13:00-13:30) using the assumption in (2.8) to estimate heading, and their estimate relative to the navsystem heading.

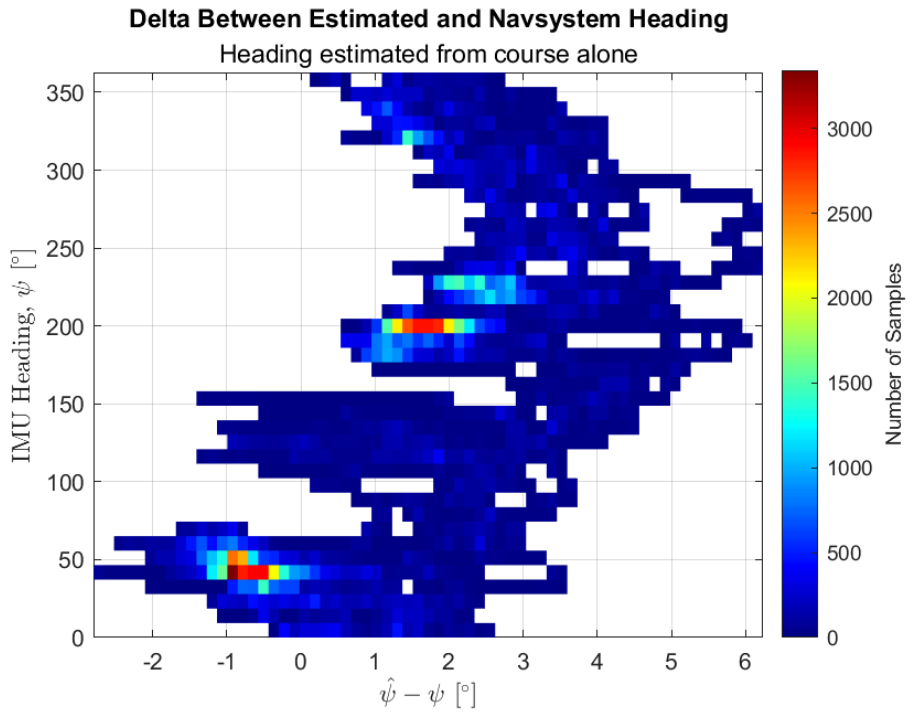

Figure 3.5 This figure shows the same data as in 3.4, with the addition of the y-axis showing navsystem heading for the samples.

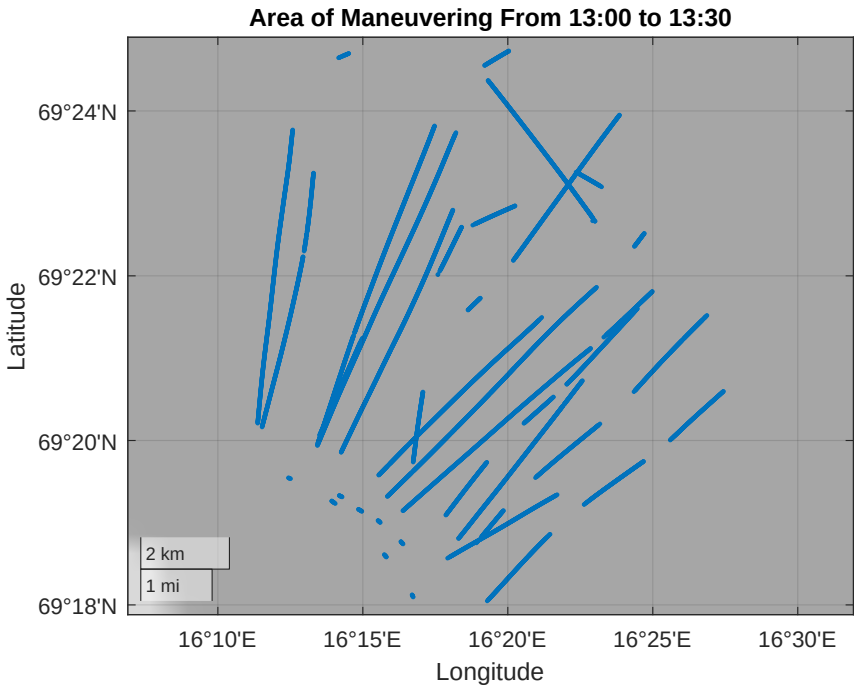

Figure 3.6 *Dataset used for wind estimation. Samples with $\left|\vec{a}_{\underline{E}B}\right| > 1\ m/s$ are excluded, giving a dataset consisting mainly of straight and level flight.*

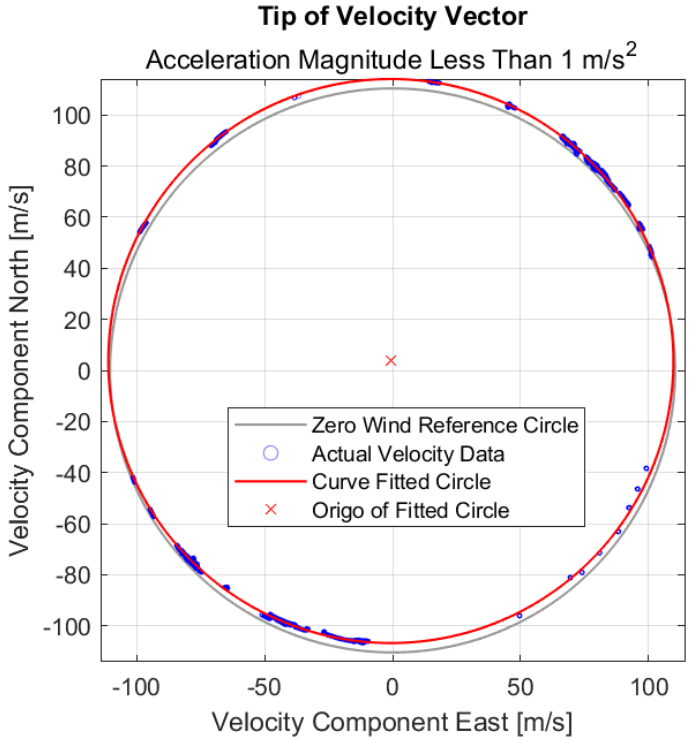

Figure 3.7 *The tip of the vectors $\mathbf{v}_{\underline{E}B}^{N}$ are plotted as blue dots. The red circle is curve fitted to the vector data.*

The histogram in figure 3.8 shows a significant tail towards positive delta heading when all samples are included. A reasonable question is why the tail in the distribution is absent on the negative side. Figure 3.9 reveals that all high g maneuvering in the dataset is related to left turns. That cause the offset in accuracy due to angle of attack to always pull the delta heading to a higher positive value, and never towards a negative value. As discussed in section 2.6.1, the angle of attack during turns will cause the heading estimate to lag the real heading, making a positive offset for left turns and a negative offset for right turns.

3.4.3 Comparing the two methods for heading estimation

Figure 3.10 shows the delta between estimated and navsystem headings for both methods discussed above, and table 3.1 summarizes mean and standard deviation. The proposed method compensates for wind, which removes the two distinct tops in the distribution of the simpler method. The standard deviation is reduced significantly for low g-samples using the proposed method, from 1.37° to 0.52°. When including all samples, the change is less, but the proposed method still gives an improvement from 1.60° to 1.10°.

		From Velocity	Proposed Method
Low G Samples	Mean [°]	0.79	0.83
	Std. [°]	1.37	0.52
All Samples	Mean [°]	1.32	1.33
	Std. [°]	1.60	1.10

Table 3.1 Mean and standard deviation of delta between estimated and navsystem heading, using velocity vector in accordance with (2.8) and the proposed method. Only samples where the g-loading was within $1 \pm 0.05g$ *are included in the "Low G Samples" rows.*

3.5 Estimating pitch

We estimated the pitch angle using the method described in section 2.7. As previously discussed, the method does not account for angle of attack. Figure 3.11 shows a significant deviation from 0° delta between estimated and navsystem pitch, even for low g-flight. The delta represents pitch for 1 g level flight.

The figure also shows a significant tail in the distribution when all samples are included, indicating a larger deviation between actual and estimated pitch angle as g-force increases.

3.6 Estimating roll

The method described in section 2.8 for estimating the roll angle is based on an assumption of coordinated flight. Coordinated flight is in general a reasonable assumption for most of the dataset at hand. However, the dataset includes some relatively heavy maneuvering, where uncoordinated flight to a certain degree is anticipated, especially when rolling into and out of steep turns.

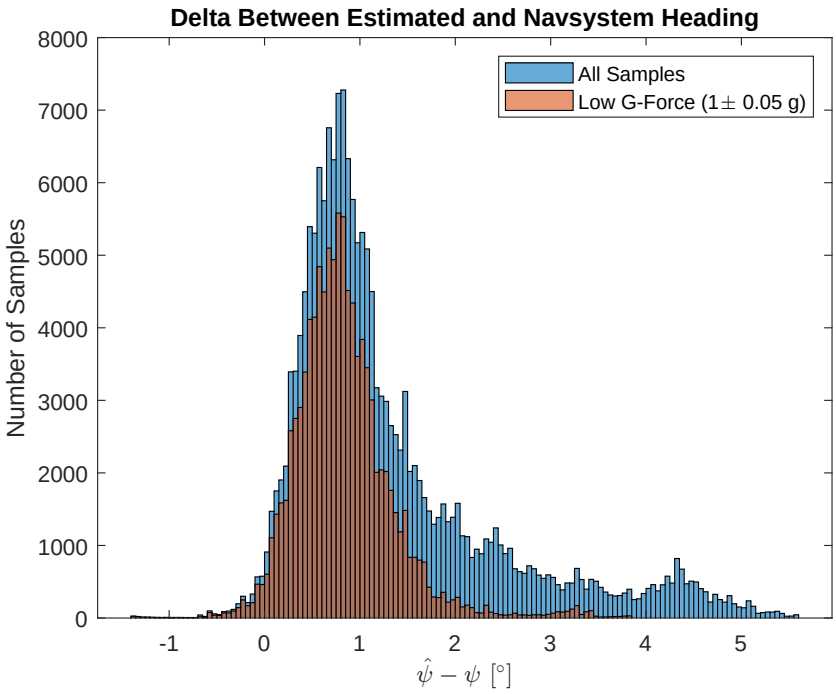

Figure 3.8 Delta between estimated and navsystem headings.

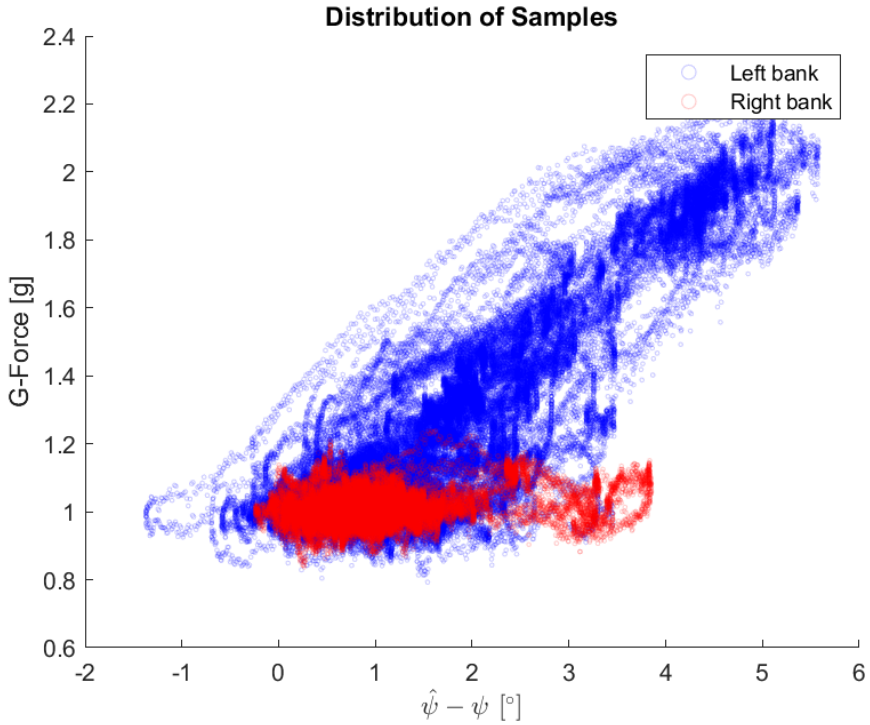

Figure 3.9 This plot shows the same data as figure 3.8, but in addition connects the distribution to the g-force along the aircraft z-axis, and right or left roll.

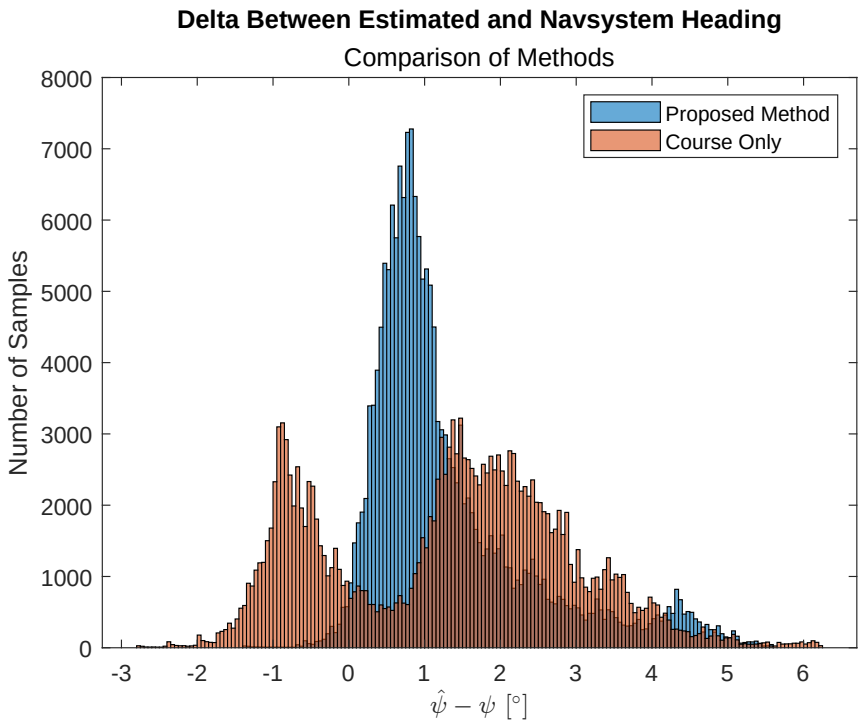

Figure 3.10 Delta between estimated and navsystem heading for the two methods.

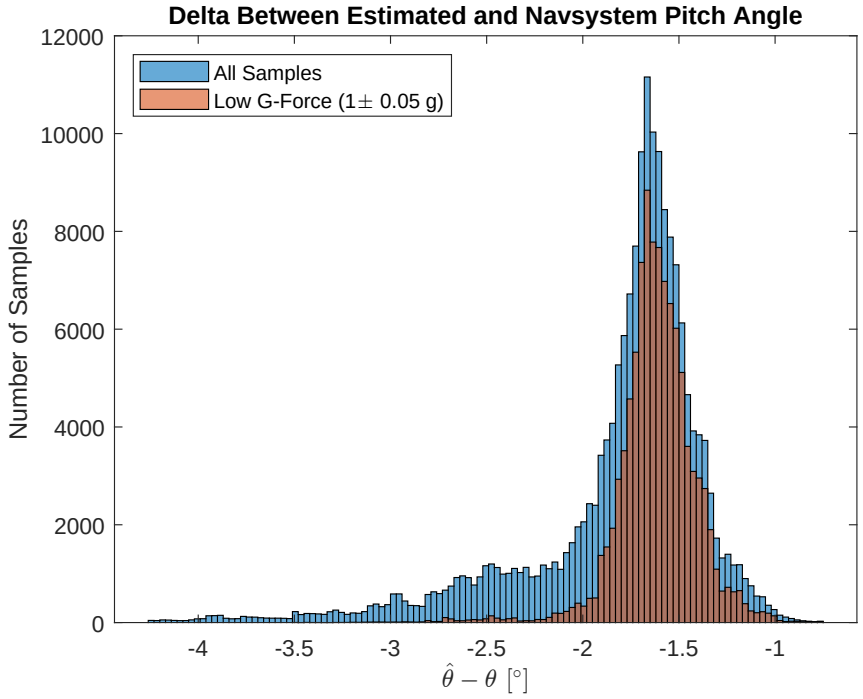

Figure 3.11 Delta between estimated and navsystem pitch angle.

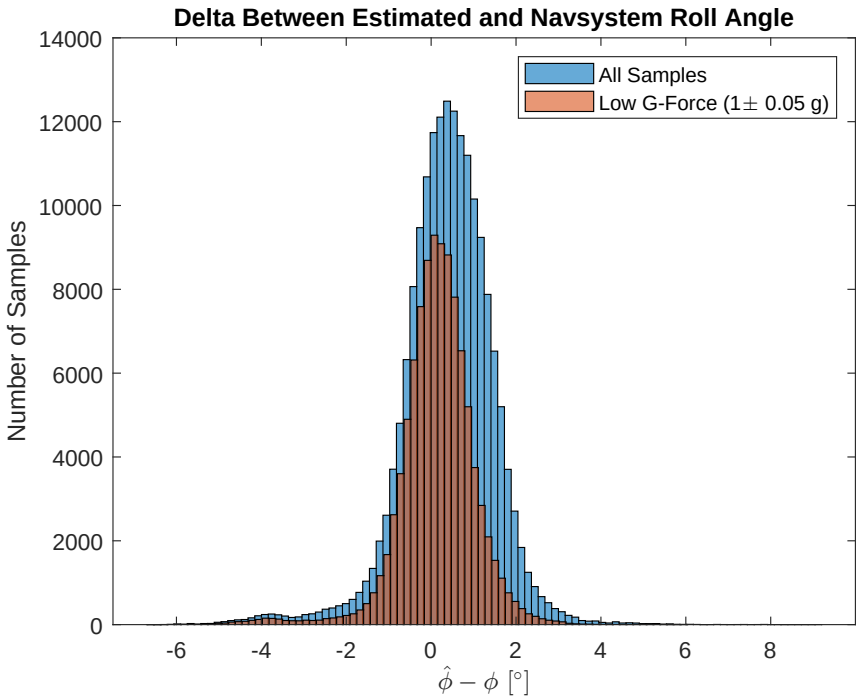

Figure 3.12 Delta between estimated and navsystem roll angle.

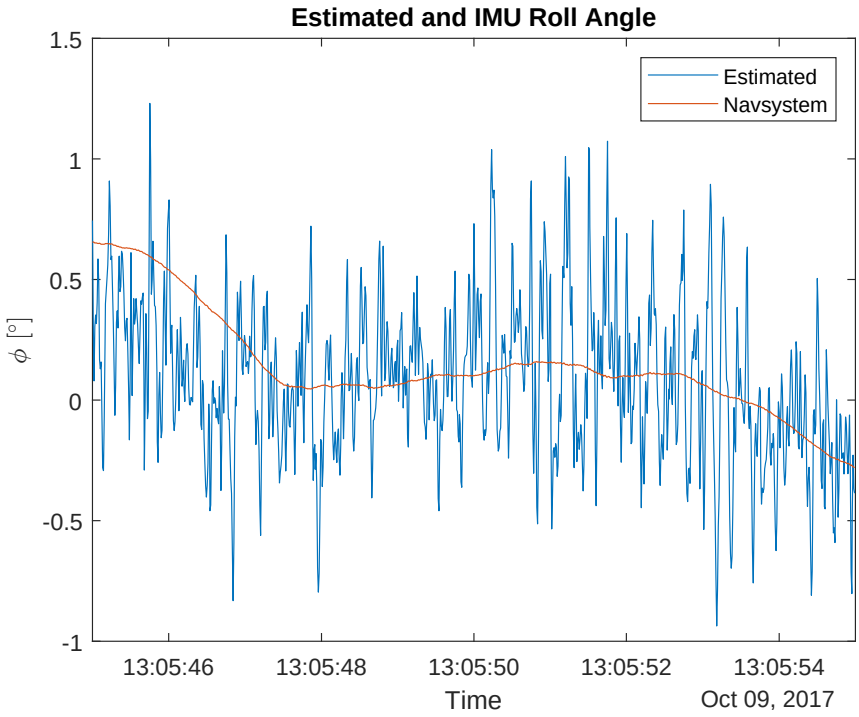

Figure 3.13 Estimated and navsystem roll angle for ten seconds in the dataset, showing how our estimate varies randomly near the navsystem value.

Figure 3.12 shows that our roll angle estimate is fairly accurate, with a mean delta between estimate and navsystem of 0.38° when including all samples. The histogram resembles a normal distribution pretty close, with a standard deviation of 1.08°. Figure 3.13 shows 10 seconds of data with roll angle close to zero, revealing a random noise in our estimate.

The method proposed for roll angle estimation is based on $\vec{a}_{\underline{E}B}$, which in our experiment is derived numerically by double differentiation of aircraft position, $\vec{p}_{EB}$. Each numerical differentiation introduces noise. That means that a higher noise component is expected in the roll angle estimation than for the pitch and heading estimates, which is based on the velocity vector $\vec{v}_{\underline{E}B}$.

Some GNSS receivers output velocity directly, by measuring the Doppler frequency shift or consecutive measurements of the carrier's phase. This enables accuracies down to a few centimeters per second [4]. Using velocity measurements instead of position measurements would probably increase the precision in the estimations, especially where double derivatives otherwise are needed like for roll angle estimation.

We did not do any smoothing on the estimates as part of the experiment, except for the optimal smoothing of the original dataset (reference orientation and position) using NavLab. The high accuracy but low precision in the roll angle estimate indicates that a proper smoothing method might increase its precision.

3.7 Compensating for angle of attack

As discussed earlier, the proposed method to attain orientation does not account for angle of attack. In some situations this leads to rather large deviations between real orientation and estimated orientation.

In this section we introduce a simple approximation to angle of attack. The purpose of introducing such a function is to see an example of how the estimation can be improved if provided with an appropriate function to estimate the angle of attack. Comparing the results to our method without angle of attack compensation also provides understanding of how the proposed method is affected by its lack of awareness for angle of attack.

3.7.1 Approximating angle of attack

For our purpose, we would like a function that outputs an estimate of the angle of attack, based on some information available in, or derivable from, $\vec{p}_{EB}$.

Let's start by a brief and simplified look at how the lift vector of an aircraft is related to angle of attack, based on [5].

L, lift, is the aerodynamic force produced by the motion of the aircraft through the air. The equation for lift is

$$L = \frac{1}{2} \cdot \rho \cdot v_{ta}^2 \cdot C_L \cdot A \tag{3.1}$$

where ρ is the density of the air, v_{ta} is the aircraft's true airspeed through the air, C_L is the lift coefficient and A is the area of the wing surface. The lift coefficient is dependent on complex relationships regarding the aircraft's shape, angle of attack and flow conditions, and is normally determined experimentally. However, for small angles the lift is directly proportional to the angle of attack.

This means that reasons for changes in angle of attack during flight could be:

- When the magnitude of the lift vector is changed, for instance
  - in a level turn.
  - when the weight of the aircraft is reduced after burning fuel.
  - when the weight of the aircraft is reduced after drop of cargo or weapons.
  - varying vertical winds/turbulence.
- When the airspeed is changed.
- When the density of the air surrounding the aircraft changes, for instance when climbing or descending.
- When the aircraft's shape is changed, for instance when changing flap position.

For the dataset in our experiment, we do not expect significant changes in air density. The airspeed was fairly constant, nothing was dropped from the aircraft and no changes was made to the aircraft configuration. That means that an approximation to angle of attack for our dataset should consider changes in the magnitude of the lift vector. Disregarding the weight change due to burned fuel through the dataset, the only factor left is the changes in the lift vector related to maneuvering, i.e. with changes in g-loading.

3.7.2 Angle of attack as a function of g-loading

Since we have reference measurements of orientation from the navsystem, we can examine the connection between g-loading and deviation between estimated and navsystem pitch angle. Figure 3.14 shows how the deviation increases with increase in g-loading for our data. The deviation is mainly due to the change in angle of attack. A simple linear approximation is shown as a yellow line, suggesting that angle of attack could be estimated as a function of g-loading by the following formula:

$$\alpha = 0.38 + 1.23g \tag{3.2}$$

If a simple approximation like (3.2) is available, valid for the dataset at hand, the orientation estimation could be improved. Since (3.2) needs an estimate of the g-loading along the aircraft z-axis, an initial estimate of the orientation is needed. The proposed method described in chapter 2, and applied on our dataset in the sections above, gives us this initial orientation enabling an estimation of aircraft g-loading from position data. The following calculations involving g-loading is based on our orientation estimate, not the orientation estimate from the navsystem.

3.7.3 Pitch angle compensated for angle of attack

To improve our estimates for pitch angle, we estimated the angle of attack for all samples according to (3.2), and added the angle of attack estimates to the original pitch estimates. The new distribution of the delta between estimated and navsystem pitch angle is shown in figure 3.15. When comparing the distribution to figure 3.11, we can see that the offset from zero delta is removed and the left tail in the distribution is mostly suppressed. As seen in table 3.2, the mean for all samples is $-0.03°$, and the standard deviation is reduced from $0.48°$ to $0.33°$.

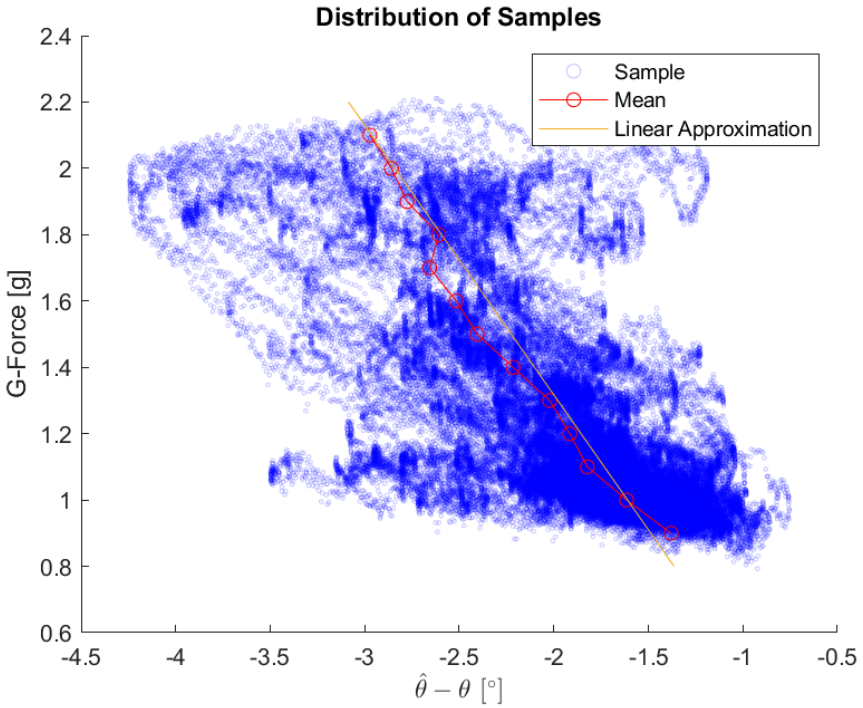

Figure 3.14 *The plot shows the connection between deviation in the estimation of pitch angle and g-loading. The red circles indicates the mean* $(\hat{\theta} - \theta)$ *for each* $0.1\ g$.

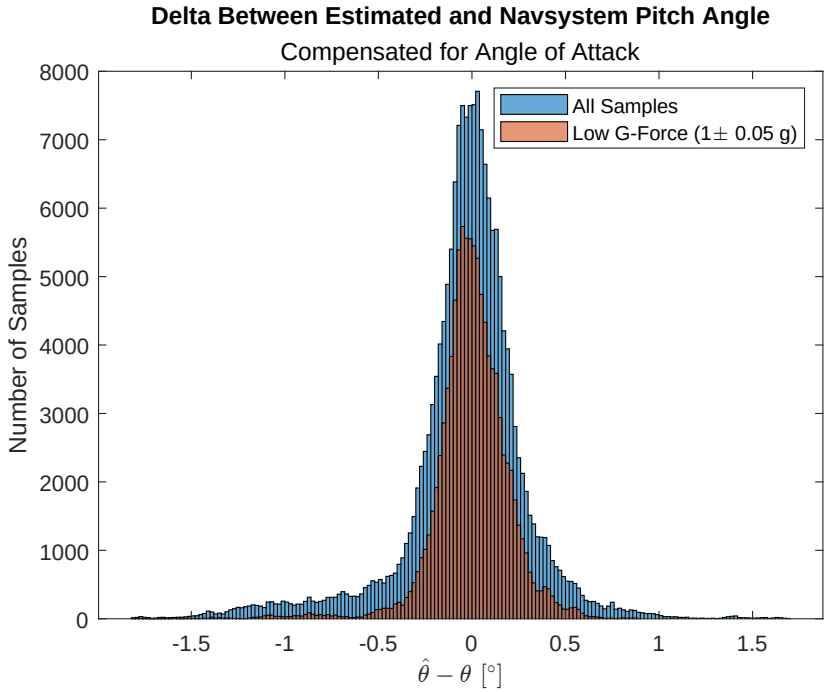

Figure 3.15 *Delta between estimated and navsystem pitch angle, when compensated for angle of attack. The shape of the distribution does not change significantly with g-loading, like it does in figure 3.11.*

		Proposed Method	With AoA Estimate
Low G Samples	Mean [°]	-1.61	-0.00
	Std. [°]	0.21	0.20
All Samples	Mean [°]	-1.81	-0.03
	Std. [°]	0.48	0.33

Table 3.2 Mean and standard deviation of delta between estimated and navsystem pitch angle, with and without compensation for angle of attack.

3.7.4 Roll angle compensated for angle of attack

We updated our estimate of the roll angle by using the original heading estimate and the updated pitch angle in 2.22 and 2.23, resulting in the distribution of delta between estimation and measurement as shown in figure 3.16. We also did a computation of the roll angle using the angle of attack-compensated heading calculated in section 3.7.5, which gave almost exactly the same result.

The shape of the distribution was only changed slightly from our old estimate, indicating that the angle of attack compensation is not necessary to make a descent roll angle estimation. Mean and standard deviation of the estimates are presented in table 3.3.

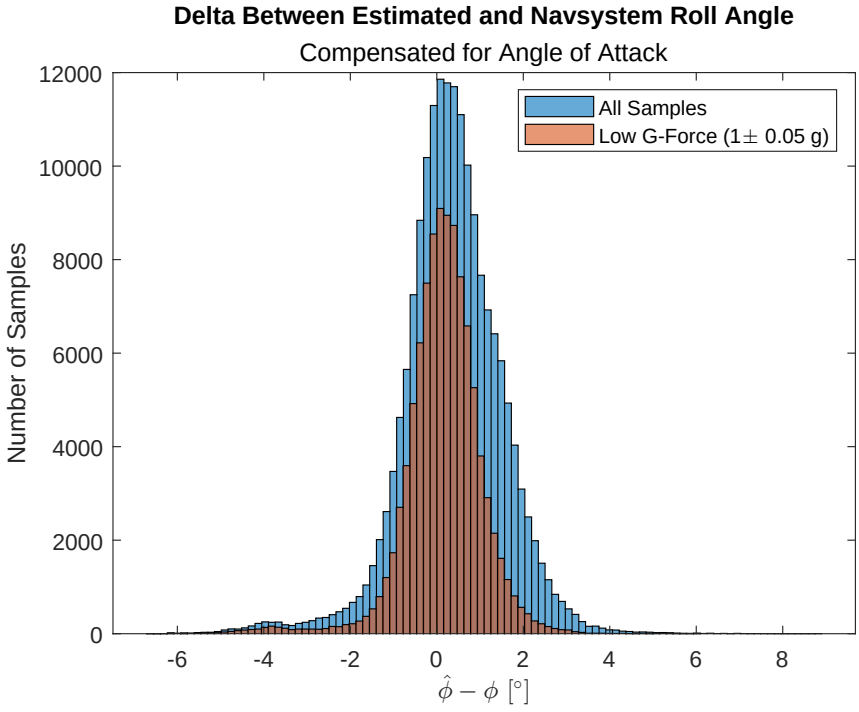

Figure 3.16 Delta between estimated and navsystem roll angle, when the pitch angle used to estimate the roll angle is compensated for angle of attack.

		Proposed Method	With AoA Estimate
Low G Samples	Mean [°]	0.14	0.14
	Std. [°]	0.90	0.91
All Samples	Mean [°]	0.38	0.35
	Std. [°]	1.08	1.16

Table 3.3 Mean and standard deviation of delta between estimated and navsystem roll angle, with and without compensation for angle of attack.

3.7.5 Heading compensated for angle of attack

To estimate an angle of attack-compensated heading, we used our initial heading estimate and added the angle of attack-component using sine to the roll angle, by the following formula:

$$\psi_{AoA\ comp.} = \psi + \alpha \cdot \sin\phi \tag{3.3}$$

Figure 3.17 shows the resulting distribution of delta between estimated and navsystem heading after compensating for angle of attack. The distinct tail on the right side of the distribution in figure 3.8 showing our original heading estimates, caused by all the hard turns in the dataset to be left turns, is suppressed even when the aircraft is maneuvering.

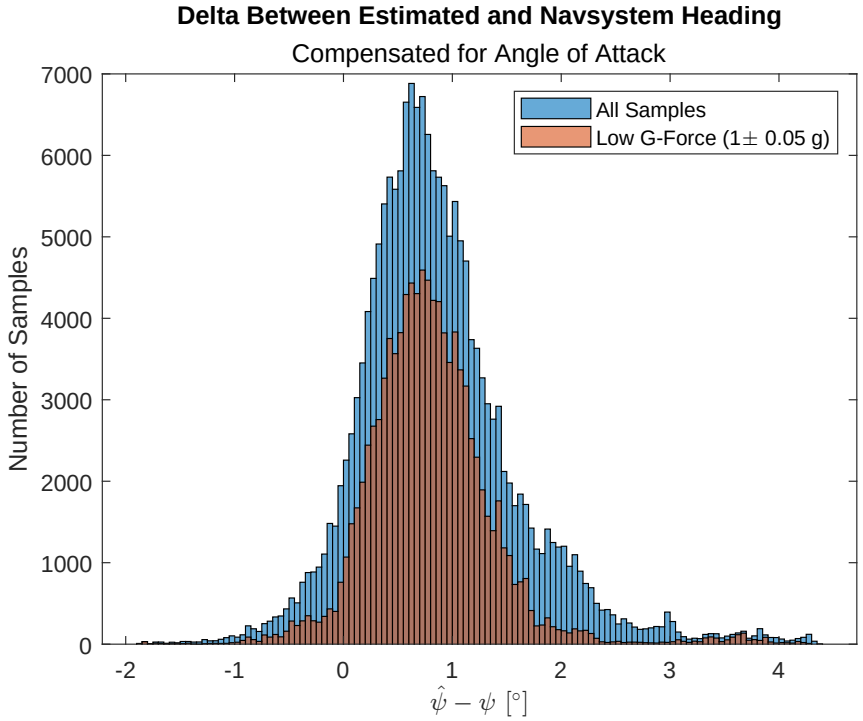

Figure 3.17 Delta between estimated and navsystem heading, when compensated for angle of attack.

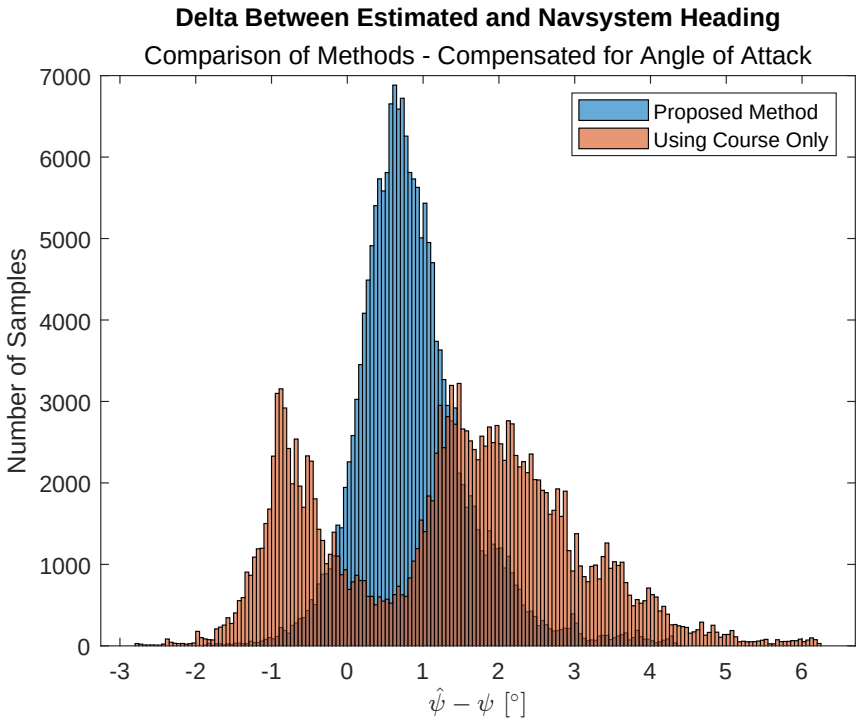

Figure 3.18 Delta between estimated and navsystem heading when using the proposed method with an angle of attack-compensation, and by using course alone, i.e. using the velocity vector in accordance with (2.8).

Figure 3.18 shows a comparison between heading estimation using the velocity vector in accordance with (2.8) and our proposed method compensated for angle of attack. Table 3.4 summarizes mean and standard deviation for delta between estimated and navsystem headings for all three estimates. The standard deviation is significantly reduced using the proposed method. The results also reveals that the standard deviation could be further decreased for maneuvering aircraft if a suitable angle of attack estimate is available.

		From Velocity	Proposed Method	With AoA Estimate
Low G Samples	Mean [°]	0.79	0.83	0.79
	Std. [°]	1.37	0.52	0.58
All Samples	Mean [°]	1.33	1.32	0.86
	Std. [°]	1.60	1.10	0.73

Table 3.4 Mean and standard deviation of delta between estimated and navsystem heading, using velocity vector in accordance with (2.8) and using the proposed method with and without compensation for angle of attack.

4 Conclusion

Chapter 2 describes a method to estimate the orientation of an aircraft on the basis of its position or velocity vector, and a number of assumptions. The method was tested on real data from a C-130J, resulting in a standard deviation between estimated and measured angle of around one degree or less for all axes. This shows that the method works, and its assumptions are reasonable for at least some practical situations.

Heading estimation using the proposed method accounts for wind, while the simpler and more common method of using the velocity vector directly under the assumption that the aircraft always points in the direction of travel, does not. The winds aloft during the experiment were calm, only about 3–4 m/s, but the improvement of the estimate was still significant.

The method was tested on position data, which were numerically differentiated to get velocity data. Numerical differentiation introduces noise in the results. The decrease in precision was significant for the roll angle estimates, which are based on double numerical differentiation to get the acceleration. If velocity data is available directly, like for a GNSS capable of measuring Doppler or carrier phase angle change, the precision could be increased.

A weakness of the method is that it does not account for the aircraft's angle of attack. Pitch angle estimates and heading estimates during maneuvering are affected by this weakness, while roll angle estimates and heading estimates during level flight is not significantly affected.

By using orientation measurements (not the estimate from our proposed method), we derived a simple approximation to angle of attack as a function of g-loading. Combining this function with the proposed method showed how the estimates could be improved if a suitable approximation is available, limiting the method's lack of precision in heading and pitch during maneuvering.

It is important that anyone that is considering to use the proposed method considers all of the underlying assumptions, and applies the method in a way that fulfills the assumptions to a reasonable extent.

References

[1] K. Gade, "Inertial navigation - theory and applications," Ph.D. dissertation, Norwegian University of Science and Technology, 2018.

[2] ——, "The seven ways to find heading," *The Journal of Navigation,* Cambridge University Press, vol. 69, no. 05, pp. 955–970, September 2016.

[3] ——, "NavLab, a generic simulation and post-processing tool for navigation," *Modeling, Identification and Control*, vol. 26, no. 03, pp. 135–150, 2005.

[4] S. Gaglione, "How does a GNSS receiver estimate velocity?" *InsideGNSS*, pp. 38–41, March/April 2015.

[5] NASA Glenn Research Center, "The beginner's guide to aeronautics," https://grc.nasa.gov/www/k-12/airplane, 2007.

About FFI

The Norwegian Defence Research Establishment (FFI) was founded 11th of April 1946. It is organised as an administrative agency subordinate to the Ministry of Defence.

FFI's mission

FFI is the prime institution responsible for defence related research in Norway. Its principal mission is to carry out research and development to meet the requirements of the Armed Forces. FFI has the role of chief adviser to the political and military leadership. In particular, the institute shall focus on aspects of the development in science and technology that can influence our security policy or defence planning.

FFI's vision

FFI turns knowledge and ideas into an efficient defence.

FFI's characteristics

Creative, daring, broad-minded and responsible.

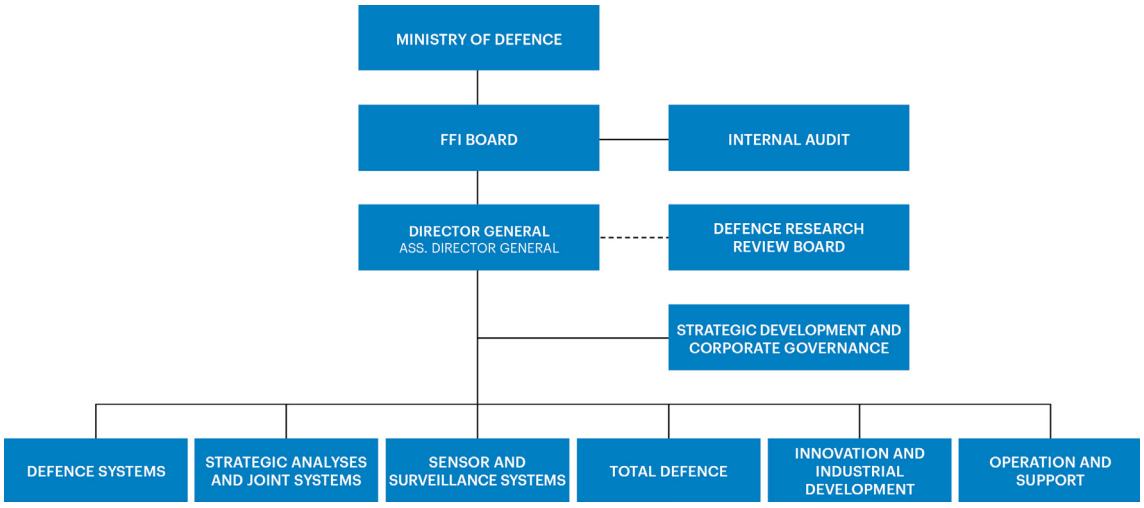

Forsvarets forskningsinstitutt (FFI)
Postboks 25
2027 Kjeller

Besøksadresse:
Kjeller: Instituttveien 20, Kjeller
Horten: Nedre vei 16, Karljohansvern, Horten

Telefon: 91 50 30 03
E-post: post@ffi.no
ffi.no

Norwegian Defence Research Establishment (FFI)
PO box 25
NO-2027 Kjeller
NORWAY

Visitor address:
Kjeller: Instituttveien 20, Kjeller
Horten: Nedre vei 16, Karljohansvern, Horten

Telephone: +47 91 50 30 03
E-mail: post@ffi.no
ffi.no/en